

Electronic States, Spin-Orbit Coupling and Magnetism in Germanium 60° Dislocations

Veronica Regazzoni, Fabrizio Rovaris, Anna Marzegalli, Francesco Montalenti, and Emilio Scalise*
Department of Materials Science, University of Milano-Bicocca, Via R. Cozzi 55, I-20125 Milano, Italy

Defects in semiconductors have recently attracted renewed interest owing to their potential in novel quantum applications. Here we investigate the electronic and magnetic properties induced by 60° dislocations in Ge. Using large-scale DFT calculations, we determine the band structure for both the shuffle and glide sets in their lowest-energy configurations. We also perform charged-defect calculations to aid in the interpretation of complex photoluminescence spectra observed in epitaxial Ge layers. The band structure for the shuffle set reveals defect-induced dispersive bands localized within the band gap near the Γ point, whereas for the glide set, we observe strong overlap with the conduction band. Defect-induced band splitting evident away from Γ reveals Rashba-Dresselhaus spin-orbit coupling, an effect previously reported only for screw dislocations. Remarkably, we find evidence that specific dislocation arrangements can stabilize antiferromagnetic ordering with sizable local magnetic moments and considerable exchange splitting between opposite spin states. These results uncover rich physics in Ge dislocations through the combination of spin-orbit coupling and magnetic ordering, potentially enabling novel defect-based functionalities in Ge devices.

Keywords: Germanium, dislocations, spin-orbit coupling, Rashba-Dresselhaus SOC, topological defects, antiferromagnetism

I. INTRODUCTION

The rise of quantum technologies in recent years has strengthened the key role of germanium (Ge) in the field of semiconductor research [1–3]. Ge is typically grown heteroepitaxially on lattice-mismatched silicon substrates, resulting in the accumulation of elastic energy and injection of line defects, known as dislocations, during the strain relaxation process [4, 5]. For a long time these defects were merely considered detrimental but, recently, defect engineering has been explored for possible applications [6–8]. The atomic structure and chemical composition of dislocation cores are critical determinants of material functionality, as they can introduce localized states within the bandgap that directly influence carrier transport, recombination dynamics, and optical absorption spectra. Dislocations exhibit remarkable parallels with low-dimensional quantum systems: their structural stability, combined with tunable electronic and spin properties, positions them as potential building blocks for emerging quantum and spintronic architectures [9–13].

The dislocations produced during the strain relaxation of epitaxial Ge layers operate on the $\{111\}\langle110\rangle$ slip system [14–16]. In particular, 60° dislocations play a prominent role, as they typically dominate the strain relaxation process. These defects have been observed and extensively characterized by experimental investigations both in constant-composition [17–20], in compositionally-graded [21, 22] and in more complex heterostructured SiGe layers [23–26]. Such dislocations belong to either glide or shuffle sets, which differ in bonding configurations and interplanar spacing, with the glide (shuffle) set consisting of closely-spaced (widely-spaced) $\{111\}$ planes. Their distinct core reconstructions have a

strong influence on the stability and electronic properties of the dislocations, motivating a focused investigation of 60° dislocations in both glide and shuffle configurations.

The quasi one-dimensional (1D) nature of dislocations and their long-range elastic interactions require large-scale simulation cells and realistic Hamiltonians to accurately model the dislocation-induced electronic states. In principle, *ab-initio* techniques such as density functional theory (DFT) are well suited for this purpose. However, standard approximations such as the local-density approximation (LDA) and the generalized gradient approximation (GGA) often fail to accurately describe the electronic bandgap of semiconductors. In fact, bulk Ge is predicted to be metallic at the LDA and GGA levels, necessitating the use of more advanced exchange-correlation functionals such as hybrid functionals (e.g., HSE06 [27, 28]) or meta-GGA functionals (e.g., mBJ [29–31]). Although these methods are computationally more demanding, they provide bandgap values closer to the experimental measurements and are essential for modeling the electronic properties of dislocations [32, 33].

In this study, we investigate the structural stability and electronic properties of the 60° perfect dislocations in Ge, considering both glide and shuffle sets. Using high-level exchange-correlation functionals and advanced atomistic modeling techniques, we aim to understand the impact of these dislocations on the electronic properties of Ge. Additionally, we investigate spin-orbit coupling effects in 60° perfect dislocations, which have been recently reported for screw dislocations in Ge [34], and we discuss the possibility of antiferromagnetic ordering in 60° perfect dislocations. Finally, we employ a transition charge model to characterize the defect levels by evaluating the total energy as a function of the Fermi level for different charge states, providing crucial information for experimental identification through spectroscopic techniques such as photoluminescence (PL). Our findings address a significant gap in the understanding of

* emilio.scalise@unimib.it

extended defects in Ge-based heterostructures and provide valuable insights for defect engineering strategies in electronic, magnetic, and spintronic device applications.

II. METHODS

We performed *ab initio* calculations within the DFT framework as implemented in the Vienna Ab initio Simulation Package (VASP) [35, 36] to investigate the electronic structure of Ge containing dislocations. Projector-augmented wave (PAW) pseudopotentials were employed, treating the $4s^24p^2$ electrons as valence, with a plane-wave energy cutoff of 250 eV. Spin-orbit coupling (SOC) was included in all calculations. To ensure a correct description of the spin-orbit splitting characteristic of Ge, calculations were also performed for primitive bulk Ge using pseudopotentials both with and without Ge 3d semi-core states, yielding no differences in the resulting spin-orbit splittings. Structural relaxations were carried out using the revised Perdew-Burke-Ernzerhof for solids (PBEsol) exchange-correlation functional [37–39]. Both atomic positions and supercell vectors were optimized until reaching an electronic energy convergence threshold of 10^{-8} eV, typically guaranteeing forces per atom below 1 meV/Å in our systems. The electronic structures were computed using the meta-GGA approach of Tran and Blaha, based on the modified Becke-Johnson (mBJ) exchange potential [29–31, 40], which has been shown to provide reasonable band gaps for bulk Ge and has been used also for other polytypes [41] and extended defects in Ge [33, 42]. Indeed, this DFT setup provides an accurate band structure at reasonable computational cost. For bulk Ge we obtained an indirect gap ($L \rightarrow \Gamma$) of 0.74 eV and a direct gap ($\Gamma \rightarrow \Gamma$) of 0.85 eV, in good agreement with the experimental values (estimated for 0K) of 0.74 eV (indirect) and 0.89 eV (direct), respectively [43, 44]. When necessary, the band structure was unfolded as described and implemented in the *fold2Bloch* software [45, 46].

The dislocation cores were modeled within periodic supercells oriented along the [121], [1̄11], and [1̄01] directions, hereafter referred to as the *x*, *y*, and *z* axes. The dislocation line is aligned along the *z* ([1̄01]) direction. Since periodic boundary conditions require a dipole configuration to compensate the Burgers vector [47], the supercell dimensions were chosen to be as large as computationally feasible to minimize the effect of the elastic interactions between dislocation cores. While fully aware of the presence of a strong elastic field in the cells, the primary concern for this study is to ensure that interactions do not significantly alter the reconstructions and the electronic properties of the dislocation cores, specifically the defect-induced energy levels within the band gap. To address this and distinguish core-specific electronic features from spurious effects, two complementary supercell arrangements were employed. The first setup consists of supercells with identical dislocation dipoles (shuf-

file–shuffle or glide–glide), while the second uses a mixed shuffle–glide dipole. The identical-dipole configuration provides a model representative of strongly coupled dislocations of the same type, capturing specific electronic and magnetic effects induced by dislocation–dislocation interactions, as analyzed below. Moreover, this setup is essential for transition charge model analysis, as the mixed configuration would yield ambiguous results due to unequal charge distribution between dissimilar cores. Conversely, the mixed dipole reduces the overlap between defect-localized wavefunctions, which would be identical and more prone to coupling in the symmetric configuration, and avoids imposing specific symmetries on the supercell. This asymmetric arrangement minimizes electronic coupling between cores, providing a more accurate model of an isolated single dislocation. The systematic comparison of results from both configurations enables the isolation of intrinsic core properties from the effects of the dipole arrangement. To our knowledge, this represents the first comprehensive use of complementary supercell models to investigate the electronic, spin, and magnetic properties of dislocation cores with this level of rigor.

Specifically, for the shuffle–shuffle dipole we used a supercell of $52.05 \times 29.52 \times 4.07$ Å (270 atoms), for the glide–glide dipole a $55.83 \times 39.63 \times 8.06$ Å (768 atoms) supercell, and for the mixed shuffle–glide dipole a $52.2 \times 29.7 \times 8.06$ Å (538 atoms) supercell, with the dislocation line along the *z*-axis. The Brillouin zone was sampled using Γ -centered *k*-points meshes of dimensions $1 \times 1 \times 4$ for the structural relaxation of the shuffle–shuffle dipole supercell, $1 \times 1 \times 2$ for the structural relaxation of the glide–glide and mixed shuffle–glide supercells and $2 \times 2 \times 12$ for the calculation of electronic properties [48].

For the thermodynamic characterization of charged defects, we employed a transition charge model by computing the formation energy of the dislocation in different charge states as a function of the Fermi level position within the bandgap [49, 50]. This approach allows the identification of thermodynamic transition levels, which can be compared with experimental spectroscopic measurements. Structural relaxations of the charged supercells were performed using the SCAN meta-generalized gradient approximation [51] within the PBE framework, due to its improved accuracy in absolute and relative energetics compared to standard GGA functionals, which is crucial for a reliable description of defect formation energies and defect level alignments in semiconductors [52–56]. Spin-orbit coupling (SOC) was included. These calculations were conducted only on supercells with shuffle–shuffle or glide–glide dipoles to avoid possible asymmetric redistribution of the charge in the mixed dipole supercell.

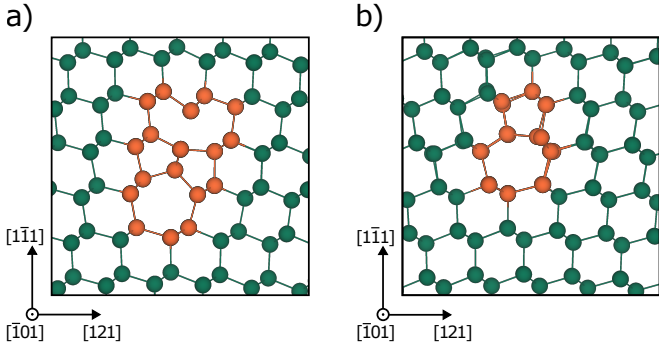


FIG. 1. a) S3 shuffle and b) glide core reconstructions of the 60° dislocation with a planar view normal to the dislocation line. Core atoms are highlighted in orange.

III. RESULTS

A. Core reconstructions of 60° dislocations

As discussed earlier, 60° dislocations in diamond-cubic semiconductors belong to two distinct structural families: the shuffle and glide sets. For the shuffle set, Pizzagalli et al. [57] proposed three possible atomic reconstructions of the dislocation core in Si, labeled S1, S2, and S3. We investigated their relative thermodynamic stability in Ge through DFT structural optimizations. The differences in core energy were evaluated as half the difference in total energy between two otherwise identical supercells containing distinct dislocation dipoles, normalized by the dislocation line length. To account for the stoichiometric difference between shuffle and glide cores, which differ by a single Ge atom per dislocation period, we corrected the total energy by subtracting the bulk Ge chemical potential, μ_{Ge} , from the glide configuration.

Our calculations show that the S1 reconstruction is unstable and spontaneously transforms into S2 upon ionic relaxation, while S2 remains stable as a local energy minimum. However, S2 lies 0.12 eV/Å higher in energy than S3 (Fig. 1a), establishing S3 as the most favorable shuffle reconstruction. Comparing the two families, the glide reconstruction (Fig. 1b) is significantly more stable than S3, with an energy difference of 1.22 eV/Å in favor of the glide configuration.

We recall that shuffle dislocations can undergo a transformation to the glide set through interaction with vacancies, which passivate dangling bonds and induce a double-periodicity reconstruction along the dislocation line [57–60]. This mechanism provides a kinetic pathway from shuffle to glide configurations. So, despite the glide configuration being much more stable in energy, we find it interesting in the following to consider also the stablest of the shuffle-set reconstruction, S3. S3 shuffle and glide reconstructions emerge indeed as the primary candidates of the 60° dislocation family to be present in epitaxial Ge layers, with the potential to significantly impact their electronic and optical properties.

B. Electronic properties and spin–orbit coupling in S3 and glide core dislocations

We now discuss the electronic properties of the S3 and glide cores. Figure 2 presents the calculated partial density of states (PDOS) and electronic band structures for both reconstructions, obtained from the mixed-dipole supercell. Since dislocations are one-dimensional crystallographic defects, fully periodic along the line direction but non-periodic in the perpendicular plane, both S3 and glide core electronic states exhibit characteristic dispersion along the Γ –X direction of the Ge Brillouin zone, which corresponds to the dislocation line orientation. The high-symmetry point of the supercell in that direction, labeled Z , is located approximately halfway along the Γ –X path.

A technical consideration arises from the structural difference between the two cores: as discussed earlier, the glide reconstruction exhibits atomic rearrangements with double periodicity compared to S3. To accommodate both core structures simultaneously, the mixed-dipole supercell adopts a doubled periodicity along the line direction and specifically, two primitive periods of S3 matching one period of the glide core. This doubling causes band folding along the Γ –Z path of the supercell reciprocal space. To facilitate interpretation, we performed an unfolding procedure to generate the bands shown in Fig. 2.

By projecting the band structure onto the core atoms of the S3 dislocation, the electronic structure reveals highly localized defect states well separated from the bulk bands and positioned deep within the Ge band gap (Fig. 2a). These states manifest as a pair of dispersive bands around the Γ point, with a dispersion spanning an energy range of 0.66 eV, particularly pronounced away from Γ where they extend below the valence-band maximum (VBM). Remarkably, while at the Γ point these bands are degenerate, they split along Γ –Z path, with a maximum splitting of 20 meV, and show opposite spin polarization, evidence of spin-orbit coupling. The spin texture analysis presented in Fig. 3 reveals a striking helical spin pattern characteristic of Rashba-Dresselhaus spin-orbit coupling (SOC). This helical texture, with spins rotating coherently around the dislocation line, is likely to originate from the screw component of the 60° dislocation, as it closely resembles the behavior reported by Liu et al. [34] for pure screw dislocations in Ge. The presence of such pronounced SOC in a mixed-character 60° dislocation demonstrates that the screw component dominates the spin physics at the shuffle core, also in the presence of an edge component.

The glide reconstruction also manifests electronic states localized at the dislocation core, but their proximity to the conduction band significantly affects their characterization (Fig. 2b). These states appear as a pair of dispersive bands positioned just below, and often overlapping with, the lowest-energy branches of the conduction band, with a dispersion extending over approximately 0.6

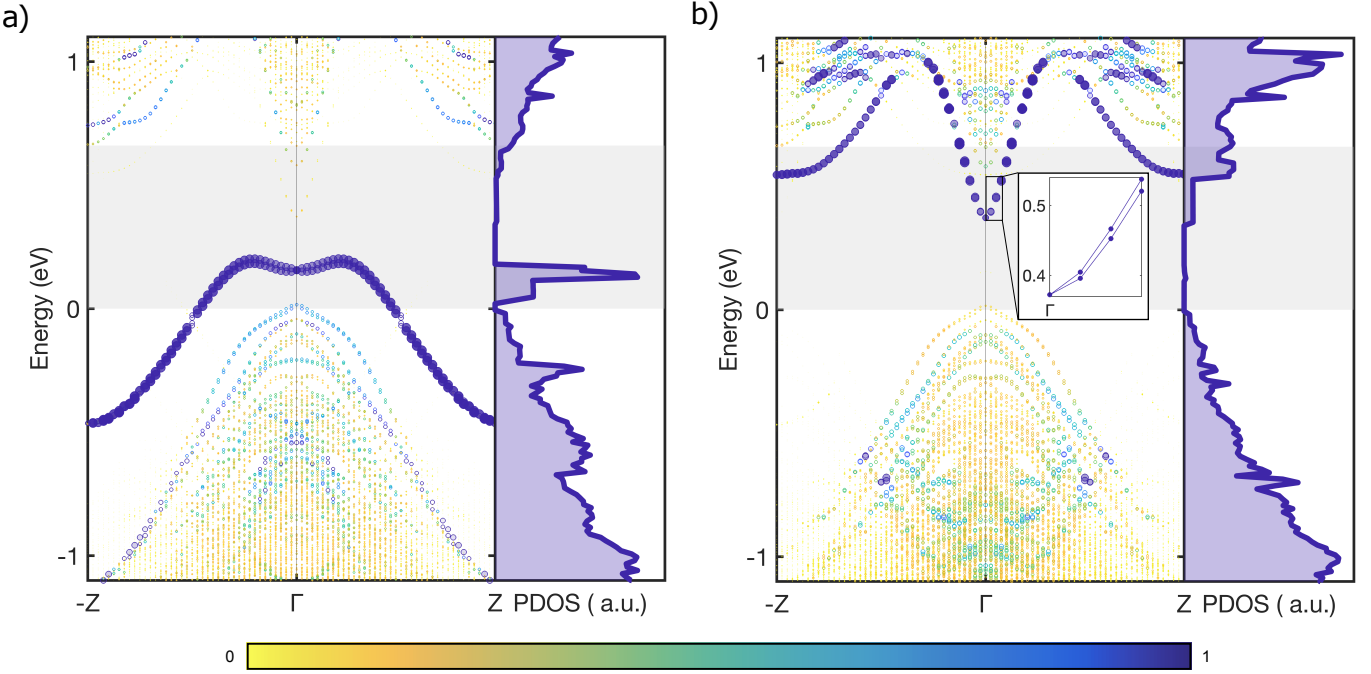


FIG. 2. Band structure and partial density of states (PDOS) of the defective supercell, projected onto the dislocation-core atoms. The band structures are plotted along the $-Z - \Gamma - Z$ path, Z being a high symmetry point in the reciprocal space of the supercell, with relative coordinates $\pm Z = (0, 0, \pm 0.5)$. Panels (a) and (b) show the unfolded band structures projected onto the shuffle S3 dislocation core atoms and glide dislocation core atoms, respectively. The color scale represents the combined weight of the band unfolding and the projection onto the dislocation core atoms, obtained through the normalized local density of states. The gray shaded region indicates the bulk Ge bandgap, with the valence-band maximum set to 0 eV. In panel (b), the inset shows a magnified view of the region delimited by the black box, where the energy splitting of the glide dislocation bands has been enhanced by a factor of three to improve visibility.

eV. In this case, the energetic splitting between the two bands due to SOC is very small, reaching a maximum of 7 meV, which makes them nearly indistinguishable within the resolution of the $Z - \Gamma - Z$ band-structure plot of Fig. 2b. This splitting is nevertheless visible in the inset, where a zoom around the Γ point clearly shows a degeneracy at Γ and an increasing energy splitting along the k path (multiplied by a factor of three to enhance visibility). This behavior suggests Rashba-Dresselhaus spin-orbit coupling (SOC) similar to that observed in the S3 shuffle core and in screw dislocations [34]. However, the strong overlap of these states with the conduction band prevents a clear resolution of the spin texture, making it far less pronounced and more difficult to isolate compared to the well-separated deep-gap states of the S3 reconstruction.

C. Magnetic ordering in shuffle S3 dislocations

The localized nature of the shuffle S3 states is further confirmed by the presence of a sharp peak in the density of states at approximately 0.13 eV above the VBM (Fig. 2a). The Fermi level in this system lies slightly above the VBM, and the corresponding dispersive bands cross both the VBM and the Fermi level, resulting in

partial filling. Charge density analysis show that these states are strongly localized at the S3 dislocation core, as illustrated in Fig. 3a. The combination of large defect-related peak in the density of states, partial band filling, and strong spatial localization provides favorable conditions for the onset of magnetic ordering. Within a simple Stoner model, when localized states cross the Fermi level with a sufficiently high density of states, the strong spatial confinement enhances the exchange interaction, and the system can spontaneously develop spin polarization: the total energy is lowered by creating an imbalance between spin-up and spin-down occupation, resulting in an exchange splitting between majority and minority spin bands [61]. The energy gain from the exchange interaction compensates for the kinetic energy cost of promoting electrons to higher-energy states, stabilizing the magnetic configuration. Similar behavior has been observed in other one-dimensional systems where localized edge or defect states at the Fermi level induce magnetic ordering, including grain boundaries in two-dimensional metal dichalcogenides [61] and zigzag edges in bismuth nanoribbons [62].

To assess the magnetic coupling between two 60° shuffle S3 dislocations, we investigated supercells containing a dipole composed of two identical shuffle dislocations. The electronic states associated with these dislocations, ob-

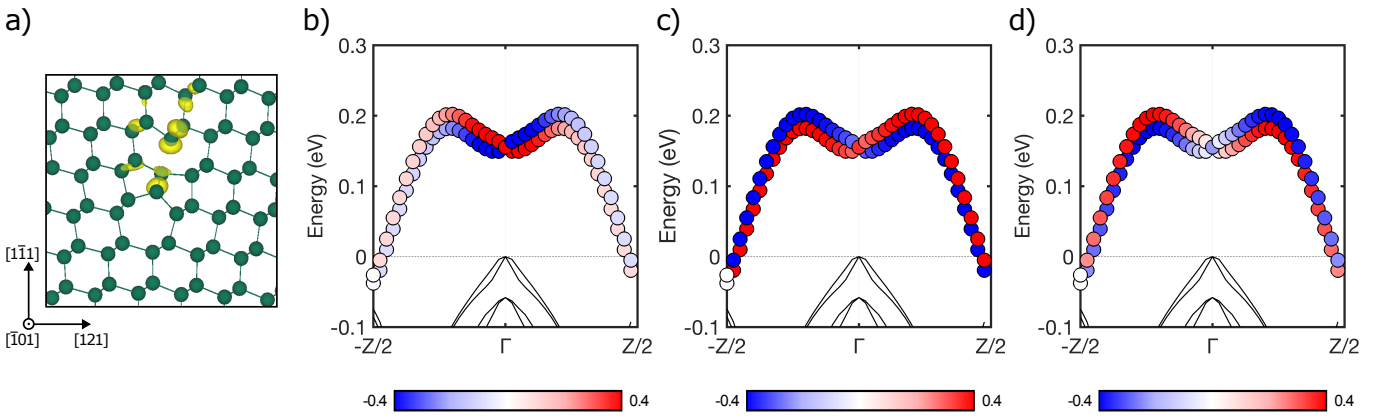


FIG. 3. a) Charge density (yellow surfaces) localization on the shuffle S3 core; b), c) and d) Spin-resolved band structure of the mixed dislocation dipole. Black solid lines denote bulk states, while dotted lines correspond to the shuffle S3 states. The color scale represents the normalized expectation values of the spin projections S_x (panel b), S_y (panel c), and S_z (panel d)

tained from both the mixed-dipole (Fig. 2a) and shuffle-shuffle dipole supercells (Fig. 4), are essentially identical in terms of dispersion, shape, and energetic position within the Ge band gap. This excellent agreement highlights the robustness of the calculated defect states with respect to the choice of supercell model.

Our calculations reveal that these dislocations can exist in two stable spin configurations, depending on the initialization of atomic magnetic moments. These configurations are either nonmagnetic (NM) or antiferromagnetic (AFM) with the NM state being energetically favored by only 1 meV per core atom. This energy difference is comparable to the convergence threshold of our calculations, indicating that the two configurations are essentially degenerate in energy. Nevertheless, the AFM configuration reveals a richer physical picture through the interplay of exchange and spin-orbit coupling. In both cases, four mid-gap bands are observed rather than the two observed in the mixed-dipole configuration, as a direct consequence of the presence of two identical dislocations in the supercell.

In the nonmagnetic configuration (Fig. 4), the four bands appear pairwise degenerate. Each pair corresponds to the spin-up and spin-down states associated with the same dislocation core, a degeneracy enforced by time-reversal symmetry T , which is preserved in the system. A small splitting between the two pairs (0.03 eV) arises from a subtle breaking of spatial inversion symmetry I .

This symmetry breaking originates from a numerical artifact inherent to the finite supercell: although the two dislocation cores are nominally identical by construction, the elastic strain fields they generate distort the supercell in such a way that, upon structural relaxation, the two cores become slightly nonequivalent. This effect is minimal, comparable to numerical noise and not discernible from the relaxed atomic structure, yet sufficient to lift the exact degeneracy between the electronic states localized on the two dislocations. Despite this small splitting, the cores remain nearly equivalent, so the defect

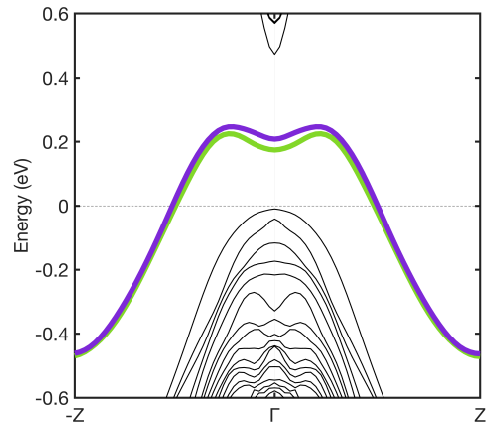


FIG. 4. Bandstructure of the nonmagnetic 60° shuffle S3 dislocation dipole. The green and purple solid lines denote two pairs of degenerate bands associated with the dislocation cores.

states form bonding- and antibonding-like combinations that are delocalized over both dislocations. The energy splitting induced by the residual inversion asymmetry is much smaller than the electronic coupling between the cores, and consequently the charge density remains substantially shared across both defects.

In the antiferromagnetic configuration (Fig. 5), time-reversal symmetry T is broken, lifting the spin degeneracy within each individual dislocation core through exchange interaction. This exchange-induced spin splitting is substantial, reaching $\Delta E_{\text{ex}} = 0.07$ eV at the Γ point, and exhibits k -dependent behavior along the Γ -Z path, reflecting the electronic structure of the localized defect states.

Remarkably, while T and I are individually broken, the combined symmetry IT remains preserved in the antiferromagnetic arrangement [62]. This combined symmetry

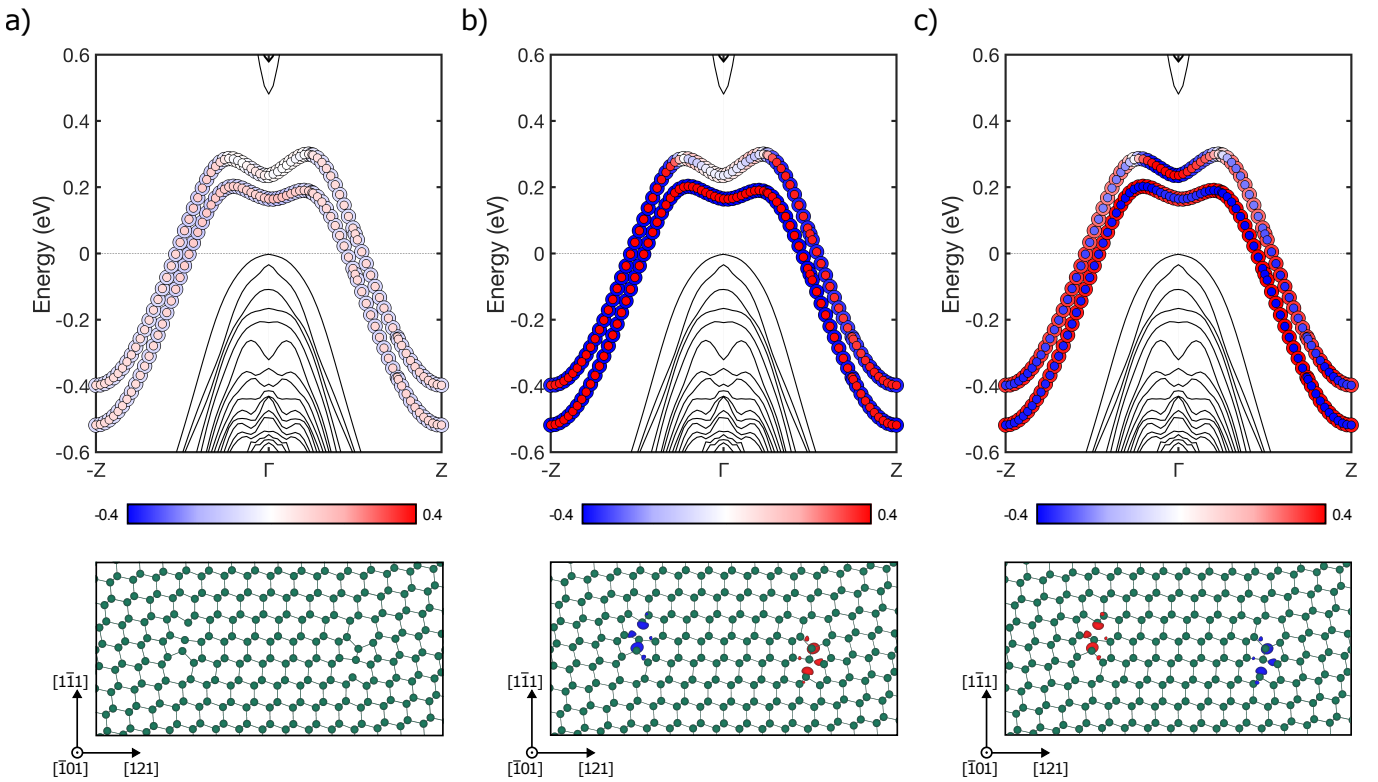


FIG. 5. Spin resolved band structures of the antiferromagnetic 60° shuffle S3 dislocation dipole. Dislocation bands are shown as circles while the bulk states are represented by the black curves. Color code represents the expectation values of the spin projections for the S_x spin projection (panel a), S_y spin projection (panel b) and S_z spin projection (panel c), with z parallel to the dislocation line. The corresponding (directional) spin densities are shown below. Blue (red) color indicates the negative (positive) isovalue in the isosurface plots.

enforces a twofold degeneracy at each k -point, effectively restoring the degeneracy between states localized on the two different dislocation cores, which was weakly broken in the nonmagnetic configuration due to the residual inversion asymmetry. In the antiferromagnetic state, this degeneracy now involves states of opposite spin on opposite cores, satisfying the relation $E(k, \uparrow, 1) = E(k, \downarrow, 2)$, where indices 1 and 2 label the two dislocations forming the dipole. Consequently, the small 0.03 eV splitting observed between core states in the nonmagnetic case vanishes in the antiferromagnetic configuration, replaced by the larger 0.07 eV exchange splitting between opposite spins on the same core. This symmetry-protected degeneracy in the antiferromagnetic state may confer enhanced robustness to the electronic structure of the dislocation cores, potentially stabilizing the defect levels against small perturbations and local disorder.

The magnetization is predominantly aligned along the y and z directions, while the x -component is negligible, as clearly shown in the spin density plots of Fig. 5. The total magnetic moment \mathbf{M} at each dislocation core is approximately $0.69 \mu_B$, indicating a substantial local spin polarization, despite the relatively small energy difference between the nonmagnetic and antiferromagnetic states. The emergence of significant local magnetic moments at

the shuffle dislocation cores, combined with the characteristic Rashba–Dresselhaus spin-orbit coupling, demonstrates that dislocations in Ge can impart qualitatively new physical properties to the material rather than simply degrading its performance. The topological stability of these extended defects, coupled with their tunable electronic and magnetic properties, makes them particularly attractive as building blocks for spintronic functionalities in Ge-based heterostructures.

D. Transition charge model and optical transition levels

To complement the electronic characterization of dislocations, we investigate their thermodynamic properties through charged-defect calculations. This approach provides valuable insights that can be compared with experimental characterization techniques. Thermodynamic transition levels, derived from the formation energies of different charge states, can be directly related to thermal ionization energies measured in deep-level transient spectroscopy (DLTS) [63, 64]. In contrast, optical transition levels, which involve electronic excitations without atomic relaxation, are relevant for comparison with

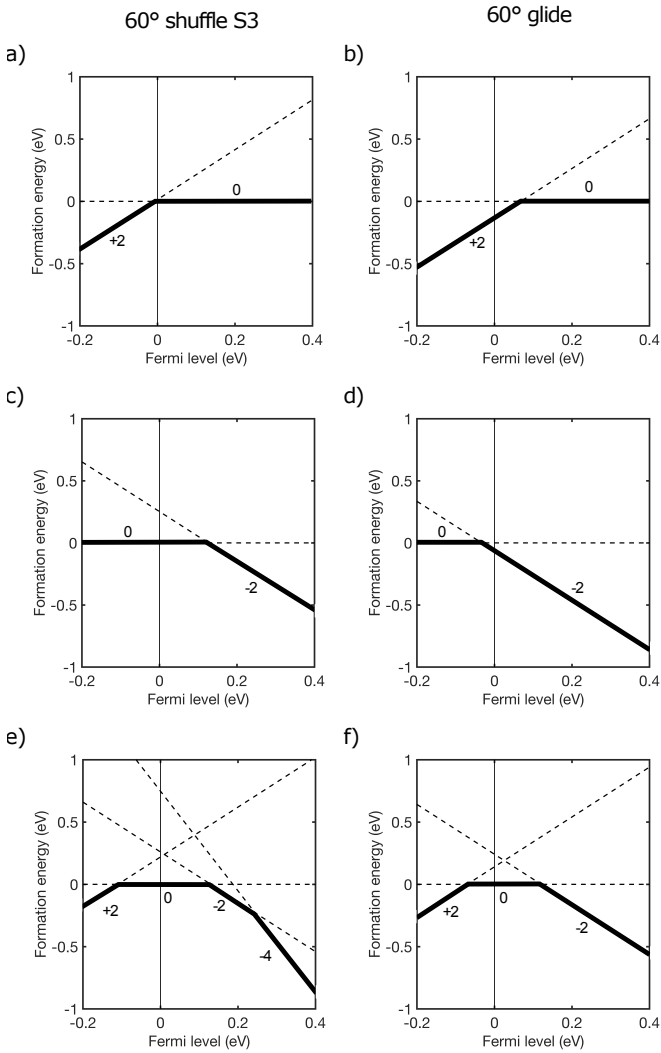


FIG. 6. Formation energy of the charged 60° dislocations as a function of Fermi energy, for both the S3 and the glide reconstructions. a), b), c) and d) cell fixed at the charged geometry (emission); e) and f) cell fixed at the neutral geometry (absorption)

PL and optical absorption measurements [64]. We focus here on optical transition levels, as PL spectroscopy is one of the most extensively employed experimental techniques for characterizing defect states in Ge epilayers grown on Si substrates [65–68]. While an accurate treatment of optically excited states would require time-dependent density-functional methods or approaches beyond DFT [64], the large system sizes required to model extended defects make such calculations computationally prohibitive. Nevertheless, the charged-defect formalism, combined with analysis of formation energies as a function of Fermi level, can provide useful indications for experimental identification and characterization of these defects.

To evaluate the formation energies of charged dislocation cores, pairs of positive or negative charges were

introduced in order to ensure equal and symmetric distribution of the charge, as required by the presence of a dislocation dipole with two identical dislocations in the simulation cell. The transition energies, defined as the charge-state transition levels, correspond to the photon energies expected to give rise to peaks in optical spectra. Both emission and absorption processes were investigated. In these simulations, we assume that the lattice does not have sufficient time to fully relax upon carrier capture or release, thus following a Franck–Condon approximation. To simulate emission, the charged structure was first fully relaxed, and the electronic charge was subsequently removed while keeping the atomic configuration fixed. Conversely, absorption was modeled by relaxing the neutral configuration and then adding the charge without further structural relaxation [64]. To ensure electrostatic neutrality in charged supercells, a homogeneous compensating background (jellium) was included as implemented in VASP. When comparing charged and neutral configurations, the resulting potential shift was corrected by aligning the electrostatic potentials in the bulk-like regions of each cell. Although additional finite-size and image-charge corrections can be applied, their impact on the present system is considered to be negligible within the scope and accuracy of the current calculations [63].

The resulting transition energies for the 60° shuffle S3 and 60° glide reconstructions are shown in Fig. 6, with the corresponding numerical values summarized in Table I. The VBM is set as the energy reference at 0 eV. For the glide reconstruction, the $(0/-2)$ absorption transition occurs at approximately 0.12 eV above the VBM, nearly identical to the corresponding transition in the shuffle reconstruction. This suggests that both dislocation cores share a common defect level at this energy, likely related to the intrinsic electronic structure of the 60° dislocation geometry. However, all other charge-state transitions for the glide reconstruction appear to be resonant with the VBM. Combined with the nonzero glide-projected DOS around the VBM (Fig. 2b), this indicates that, apart from the single transition at 0.12 eV, the glide dislocation does not introduce additional well-defined localized deep states within the bandgap. In contrast, the shuffle (S3) reconstruction exhibits an additional distinct transition level at approximately 0.25 eV above the VBM for the $(-2/-4)$ absorption process. The presence of this deeper level, associated with the second defect-related dispersive band visible in Fig. 2a, distinguishes the shuffle reconstruction and makes it more optically active than the glide.

A direct quantitative comparison between our calculated optical-transition energies and experimental PL measurements is challenging for several reasons. First, the inherent accuracy limitations of DFT-based calculations, as explained above. More importantly, epitaxial Ge layers probed experimentally are considerably more complex than our idealized models: they typically contain multiple types of dislocations (not only 60° but likely

other dislocations and extended defects), point defects (vacancies, interstitials, impurities), and their mutual interactions, all of which can contribute to the PL spectrum. Despite these complexities, our calculated optical-transition energies for 60° dislocations in Ge fall within the range of experimentally observed PL features [65–68], demonstrating consistency between theory and experiment. These results therefore provide an essential piece of the puzzle that, combined with past and future computational and experimental studies, will enable a comprehensive interpretation of the rich PL spectra observed in epitaxial Ge layers.

	60° shuffle S3	60° glide
(+2/0) emission	-0.01 eV	0.07 eV
(0/-2) emission	0.12 eV	-0.03 eV
(+2/0) absorption	-0.11 eV	-0.07 eV
(0/-2) absorption	0.13 eV	0.12 eV
(-2/-4) absorption	0.25 eV	–

TABLE I. Transition energies for the charged 60° dislocation in both S3 and glide reconstructions.

IV. CONCLUSIONS

In summary, we present a comprehensive first-principles investigation of the structural stability and electronic properties of 60° perfect dislocations in germanium, considering both glide-set and shuffle-set reconstructions. Our DFT calculations using the mBJ meta-GGA functional reveal that the electronic properties of these two reconstructions differ markedly. The glide reconstruction exhibits a nearly bulk-like electronic character with dislocation-induced states that overlap strongly with the valence band, resulting in minor perturbation of the Ge band structure. In contrast, the shuffle S3 reconstruction introduces two highly localized, dispersive bands within the Ge bandgap, positioned approximately 0.13 eV above the VBM. These localized states cross the Fermi level and exhibit substantial spin-orbit coupling effects, displaying characteristic Rashba-Dresselhaus helical spin textures analogous to those reported for screw dislocations.

The combination of large defect-related peak in the density of states lying close to the Fermi level and strong spatial localization of the defect states provides favorable conditions for magnetic ordering through a Stoner-like mechanism. In the shuffle-shuffle dipole configuration, we find that the system can stabilize an antiferromagnetic state with local magnetic moments of approximately $0.69 \mu_B$ per dislocation core and an ex-

change splitting of $\Delta E_{\text{ex}} = 0.07$ eV between opposite spin states. Notably, the antiferromagnetic configuration restores the exact degeneracy between electronic states localized on the two dislocation cores through combined inversion-time-reversal (IT) symmetry, a degeneracy that was weakly broken in the nonmagnetic state due to residual strain-induced asymmetry in the finite supercell. This symmetry-enforced degeneracy suggests that the electronic states of coupled identical dislocation cores may exhibit enhanced robustness against local perturbations and structural disorder, potentially providing intrinsic stability to the spin-polarized defect levels against environmental fluctuations.

These results demonstrate that dislocations in Ge can impart qualitatively new physical properties, such as intrinsic magnetism, spin-orbit-coupled electronic states, and topological spin textures, rather than simply degrading material performance. The topological stability of these extended defects, coupled with their tunable electronic and magnetic properties, positions them as promising building blocks for spintronic functionalities in Ge-based heterostructures.

Finally, through charged-defect calculations, we identify optical transition levels that can guide experimental identification via photoluminescence spectroscopy. Both glide and shuffle reconstructions share a common transition level at approximately 0.13 eV above the VBM, likely related to the intrinsic 60° dislocation geometry. However, the shuffle reconstruction exhibits an additional deeper level at 0.23 eV, making it significantly more optically active than the glide reconstruction.

These findings highlight the crucial role of core reconstructions in dictating the functional properties of dislocations in germanium. Our results address a significant gap in understanding extended defects in Ge and demonstrate that careful control of dislocations core structure can enable novel quantum and spintronic functionalities in this technologically relevant semiconductor platform.

ACKNOWLEDGEMENTS

The authors acknowledge the CINECA consortium under the ISCRA initiative for the availability of high-performance computing resources and support.

F.M. acknowledges financial support by the European Union – NextGenerationEU – Investment 1.1, M4C2 - Project Title “NANOSEES” n. P2022YM8J3 – CUP D53D23018720001 - Grant Assignment Decree No. 1389 adopted on 1st September 2023 by the Italian Ministry of University and Research (MUR).

[1] G. Scappucci, C. Kloeffel, F. A. Zwanenburg, D. Loss, M. Myronov, J.-J. Zhang, S. De Franceschi, G. Katsaros,

and M. Veldhorst, The germanium quantum information route, *Nature Reviews Materials* **6**, 926 (2021).

- [2] T. Koch, C. Godfrin, V. Adam, J. Ferrero, D. Schroller, N. Glaeser, S. Kubicek, R. Li, R. Loo, S. Massar, G. Simion, D. Wan, K. De Greve, and W. Wernsdorfer, Industrial 300 mm wafer processed spin qubits in natural silicon/silicon-germanium, *npj Quantum Information* **11**, 59 (2025).
- [3] Y. Shimura, C. Godfrin, A. Hikavyy, R. Li, J. Aguilera, G. Katsaros, P. Favia, H. Han, D. Wan, K. De Greve, and R. Loo, Compressively strained epitaxial ge layers for quantum computing applications, *Materials Science in Semiconductor Processing* **174**, 108231 (2024).
- [4] J. W. Matthews and A. E. Blakeslee, Defects in epitaxial multilayers: I. Misfit dislocations, *Journal of Crystal Growth* **27**, 118 (1974).
- [5] R. People and J. C. Bean, Calculation of critical layer thickness versus lattice mismatch for Ge_xSi_{1-x}/Si strained-layer heterostructures, *Applied Physics Letters* **47**, 322 (1985).
- [6] V. Ivády, J. Davidsson, N. Delegan, A. L. Falk, P. V. Klimov, S. J. Whiteley, S. O. Hruszkewycz, M. V. Holt, F. J. Heremans, N. T. Son, *et al.*, Stabilization of point-defect spin qubits by quantum wells, *Nature communications* **10**, 5607 (2019).
- [7] D. Barragan-Yani and L. Wirtz, Assessing the potential of perfect screw dislocations in SiC for solid-state quantum technologies, *Physical Review Research* **6**, L022055 (2024).
- [8] J. A. Steele, P. J. Strohbeen, C. Verdi, A. Baktash, A. Danilenko, Y.-H. Chen, J. van Dijk, F. H. Knudsen, A. Leblanc, D. Perconte, *et al.*, Superconductivity in substitutional ga-hyperdoped ge epitaxial thin films, *Nature Nanotechnology* , 1 (2025).
- [9] S. Polat Genlik, R. C. Myers, and M. Ghazisaeidi, Dislocations as natural quantum wires in diamond, *Physical Review Materials* **7**, 024601 (2023).
- [10] V. Krivobok, S. Nikolaev, S. Chentsov, E. Onishchenko, A. Pruchkina, V. Bagaev, A. Silina, and N. Smirnova, Two types of isolated (quantum) emitters related to dislocations in crystalline cdznte, *Journal of Luminescence* **200**, 240 (2018).
- [11] X. Li, B. Han, R. Zhu, R. Shi, M. Wu, Y. Sun, Y. Li, B. Liu, L. Wang, J. Zhang, *et al.*, Dislocation-tuned ferroelectricity and ferromagnetism of the bfeo₃/srruo₃ interface, *Proceedings of the National Academy of Sciences* **120**, e2213650120 (2023).
- [12] Y. Liang, D. Yi, T. Nan, S. Liu, L. Zhao, Y. Zhang, H. Chen, T. Xu, M. Dai, J.-M. Hu, *et al.*, Field-free spin-orbit switching of perpendicular magnetization enabled by dislocation-induced in-plane symmetry breaking, *Nature Communications* **14**, 5458 (2023).
- [13] C. Zhang, V. W.-z. Yu, Y. Jin, J. Nagura, S. P. Genlik, M. Ghazisaeidi, and G. Galli, Towards dislocation-driven quantum interconnects, *npj Computational Materials* **10.1038/s41524-025-01945-3** (2026).
- [14] E. A. Fitzgerald Jr, *The properties, control and elimination of misfit dislocations in semiconductor heterostructures* (Cornell University, 1989).
- [15] J. P. Hirth, J. Lothe, and T. Mura, Theory of dislocations, *Journal of Applied Mechanics* **50**, 476 (1983).
- [16] P. Humble and R. Hannink, Plastic deformation of diamond at room temperature, *Nature* **273**, 37 (1978).
- [17] P. Mooney, Strain relaxation and dislocations in sige/si structures, *Materials Science and Engineering: R: Reports* **17**, 105 (1996).
- [18] Y. B. Bolkhovityanov and L. V. Sokolov, Ge-on-si films obtained by epitaxial growing: edge dislocations and their participation in plastic relaxation, *Semiconductor Science and Technology* **27**, 043001 (2012).
- [19] F. Rovaris, M. H. Zoellner, P. Zaumseil, M. A. Schubert, A. Marzegalli, L. Di Gaspare, M. De Seta, T. Schroeder, P. Storck, G. Schwalb, C. Richter, T. U. Schülli, G. Capellini, and F. Montalenti, Misfit-dislocation distributions in heteroepitaxy: From mesoscale measurements to individual defects and back, *Phys. Rev. Appl.* **10**, 054067 (2018).
- [20] A. Marzegalli, M. Brunetto, M. Salvalaglio, F. Montalenti, G. Nicotra, M. Scuderi, C. Spinella, M. De Seta, and G. Capellini, Onset of plastic relaxation in the growth of ge on si(001) at low temperatures: Atomic-scale microscopy and dislocation modeling, *Physical Review B* **88**, 165418 (2013).
- [21] F. K. LeGoues, B. S. Meyerson, and J. F. Morar, Anomalous strain relaxation in sige thin films and superlattices, *Phys. Rev. Lett.* **66**, 2903 (1991).
- [22] T. Wang, Y. Zhang, and S. Chua, Dislocation evolution in epitaxial multilayers and graded composition buffers, *Acta Materialia* **49**, 1599 (2001).
- [23] E. A. Fitzgerald, M. T. Currie, S. B. Samavedam, T. A. Langdo, G. Taraschi, V. Yang, C. W. Leitz, and M. T. Bulsara, Dislocations in relaxed sige/si heterostructures, *physica status solidi (a)* **171**, 227 (1999).
- [24] O. Skibitzki, M. H. Zoellner, F. Rovaris, M. A. Schubert, Y. Yamamoto, L. Persichetti, L. Di Gaspare, M. De Seta, R. Gatti, F. Montalenti, and G. Capellini, Reduction of threading dislocation density beyond the saturation limit by optimized reverse grading, *Phys. Rev. Mater.* **4**, 103403 (2020).
- [25] R. D. Arroyo, F. Isa, G. Isella, R. Erni, H. von Känel, P. Gröning, and M. D. Rossell, Effect of thermal annealing on the interface quality of ge/si heterostructures, *Scripta Materialia* **170**, 52 (2019).
- [26] F. Rovaris, F. Isa, R. Gatti, A. Jung, G. Isella, F. Montalenti, and H. von Känel, Three-dimensional sige/si heterostructures: Switching the dislocation sign by substrate under-etching, *Physical Review Materials* **1**, 073602 (2017).
- [27] J. Heyd, G. E. Scuseria, and M. Ernzerhof, Hybrid functionals based on a screened coulomb potential, *The Journal of chemical physics* **118**, 8207 (2003).
- [28] J. E. Peralta, J. Heyd, G. E. Scuseria, and R. L. Martin, Spin-orbit splittings and energy band gaps calculated with the heyd-scuseria-ernzerhof screened hybrid functional, *Physical Review B—Condensed Matter and Materials Physics* **74**, 073101 (2006).
- [29] A. D. Becke and E. R. Johnson, A simple effective potential for exchange, *The Journal of chemical physics* **124** (2006).
- [30] F. Tran, P. Blaha, and K. Schwarz, Band gap calculations with becke-johnson exchange potential, *Journal of Physics: Condensed Matter* **19**, 196208 (2007).
- [31] F. Tran and P. Blaha, Accurate band gaps of semiconductors and insulators with a semilocal exchange-correlation potential, *Physical review letters* **102**, 226401 (2009).
- [32] E. Scalise, L. Barbisan, A. Sarikov, F. Montalenti, L. Miglio, and A. Marzegalli, The origin and nature of killer defects in 3C-SiC for power electronic applications by a multiscale atomistic approach, *Journal of Materials Chemistry C* **8**, 8380 (2020), arXiv:2001.11826.

- [33] E. M. Fadaly, A. Marzegalli, Y. Ren, L. Sun, A. Dijkstra, D. De Matteis, E. Scalise, A. Sarikov, M. De Luca, R. Rurrali, I. Zardo, J. E. Haverkort, S. Botti, L. Miglio, E. P. Bakkers, and M. A. Verheijen, Unveiling Planar Defects in Hexagonal Group IV Materials, *Nano Letters* **21**, 3619 (2021).
- [34] L. Hu, H. Huang, Z. Wang, W. Jiang, X. Ni, Y. Zhou, V. Zielasek, M. Lagally, B. Huang, and F. Liu, Ubiquitous spin-orbit coupling in a screw dislocation with high spin coherency, *Physical review letters* **121**, 066401 (2018).
- [35] G. Kresse and J. Furthmüller, Efficient iterative schemes for ab initio total-energy calculations using a plane-wave basis set, *Physical review B* **54**, 11169 (1996).
- [36] G. Kresse and J. Furthmüller, Efficiency of ab-initio total energy calculations for metals and semiconductors using a plane-wave basis set, *Computational materials science* **6**, 15 (1996).
- [37] J. P. Perdew, A. Ruzsinszky, G. I. Csonka, O. A. Vydrov, G. E. Scuseria, L. A. Constantin, X. Zhou, and K. Burke, Restoring the density-gradient expansion for exchange in solids and surfaces, *Physical review letters* **100**, 136406 (2008).
- [38] G. I. Csonka, J. P. Perdew, A. Ruzsinszky, P. H. Philipsen, S. Lebègue, J. Paier, O. A. Vydrov, and J. G. Ángyán, Assessing the performance of recent density functionals for bulk solids, *Physical Review B—Condensed Matter and Materials Physics* **79**, 155107 (2009).
- [39] G.-X. Zhang, A. M. Reilly, A. Tkatchenko, and M. Scheffler, Performance of various density-functional approximations for cohesive properties of 64 bulk solids, *New Journal of Physics* **20**, 063020 (2018).
- [40] J. P. Perdew, A. Ruzsinszky, J. Tao, V. N. Staroverov, G. E. Scuseria, and G. I. Csonka, Prescription for the design and selection of density functional approximations: More constraint satisfaction with fewer fits, *The Journal of chemical physics* **123** (2005).
- [41] C. Rödl, J. Furthmüller, J. R. Suckert, V. Armuzza, F. Bechstedt, and S. Botti, Accurate electronic and optical properties of hexagonal germanium for optoelectronic applications, *Physical Review Materials* **3**, 034602 (2019), [arXiv:1812.01865](https://arxiv.org/abs/1812.01865).
- [42] A. Marzegalli, F. Montalenti, and E. Scalise, Polytypic quantum wells in si and ge: impact of 2d hexagonal inclusions on electronic band structure, *Nanoscale Horiz.* **9**, 2320 (2024).
- [43] C. Kittel, *Introduction to Solid State Physics*, 8th ed. (John Wiley & Sons, Hoboken, NJ, 2005).
- [44] Ioffe Institute, *Band structure and carrier concentration of Germanium (Ge)*, NSM Archive - Physical Properties of Semiconductors, accessed: 2026.
- [45] O. Rubel, A. Bokhanchuk, S. Ahmed, and E. Assmann, Unfolding the band structure of disordered solids: From bound states to high-mobility kane fermions, *Physical Review B* **90**, 115202 (2014).
- [46] L.-W. Wang, L. Bellaiche, S.-H. Wei, and A. Zunger, “majority representation” of alloy electronic states, *Physical review letters* **80**, 4725 (1998).
- [47] W. Cai, V. V. Bulatov, J. Chang, J. Li, and S. Yip, Anisotropic elastic interactions of a periodic dislocation array, *Physical Review Letters* **86**, 5727 (2001).
- [48] H. J. Monkhorst and J. D. Pack, Special points for brillouin-zone integrations, *Physical review B* **13**, 5188 (1976).
- [49] P. Śpiewak, K. Sueoka, J. Vanhellemont, K. Kurzydłowski, K. Młynarczyk, P. Wabiński, and I. Romandic, Ab initio calculation of the formation energy of charged vacancies in germanium, *Physica B: Condensed Matter* **401**, 205 (2007).
- [50] E. Degoli, R. Guerra, F. Iori, R. Magri, I. Marri, O. Pulci, O. Bisi, and S. Ossicini, Ab-initio calculations of luminescence and optical gain properties in silicon nanostructures, *Comptes Rendus. Physique* **10**, 575 (2009).
- [51] J. Sun, A. Ruzsinszky, and J. P. Perdew, Strongly constrained and appropriately normed semilocal density functional, *Physical review letters* **115**, 036402 (2015).
- [52] P. Borlido, T. Aull, A. W. Huran, F. Tran, M. A. Marques, and S. Botti, Large-scale benchmark of exchange-correlation functionals for the determination of electronic band gaps of solids, *Journal of chemical theory and computation* **15**, 5069 (2019).
- [53] M. Kothakonda, A. D. Kaplan, E. B. Isaacs, C. J. Bartel, J. W. Furness, J. Ning, C. Wolverton, J. P. Perdew, and J. Sun, Testing the r2scan density functional for the thermodynamic stability of solids with and without a van der waals correction, *ACS Materials Au* **3**, 102 (2022).
- [54] Y. Zhang, D. A. Kitchev, J. Yang, T. Chen, S. T. Dacek, R. A. Sarmiento-Pérez, M. A. Marques, H. Peng, G. Ceder, J. P. Perdew, *et al.*, Efficient first-principles prediction of solid stability: Towards chemical accuracy, *npj Computational Materials* **4**, 9 (2018).
- [55] M. Maciaszek, V. Žalandauskas, R. Silkinis, A. Alkauskas, and L. Razinkovas, The application of the scan density functional to color centers in diamond, *The Journal of Chemical Physics* **159** (2023).
- [56] A. V. Ivanov, Y. L. Schmerwitz, G. Levi, and H. Jónsson, Electronic excitations of the charged nitrogen-vacancy center in diamond obtained using time-independent variational density functional calculations, *SciPost Physics* **15**, 009 (2023).
- [57] L. Pizzagalli, J. Godet, J. Guénolé, and S. Brochard, Dislocation cores in silicon: new aspects from numerical simulations, in *Journal of Physics: Conference Series*, Vol. 281 (IOP Publishing, 2011) p. 012002.
- [58] J. Hornstra, Dislocations in the diamond lattice, *Journal of Physics and Chemistry of Solids* **5**, 129 (1958).
- [59] D. Hull and D. J. Bacon, *Introduction to dislocations*, Vol. 37 (Elsevier, 2011).
- [60] L. Barbisan, A. Marzegalli, and F. Montalenti, Atomic-scale insights on the formation of ordered arrays of edge dislocations in ge/si (001) films via molecular dynamics simulations, *Scientific Reports* **12**, 3235 (2022).
- [61] Z. Zhang, X. Zou, V. H. Crespi, and B. I. Yakobson, Intrinsic magnetism of grain boundaries in two-dimensional metal dichalcogenides, *ACS Nano* **7**, 10475 (2013).
- [62] I. I. Naumov and P. Dev, One-dimensional magnetism and rashba-like effects in zigzag bismuth nanoribbons, *Physical Review Materials* **7**, 026204 (2023).
- [63] J. Weber, A. Janotti, and C. Van de Walle, Dangling bonds and vacancies in germanium, *Physical Review B—Condensed Matter and Materials Physics* **87**, 035203 (2013).
- [64] C. Freysoldt, B. Grabowski, T. Hickel, J. Neugebauer, G. Kresse, A. Janotti, and C. G. Van de Walle, First-principles calculations for point defects in solids, *Reviews of Modern Physics* **86**, 253 (2014).

- [65] T. Arguirov, M. Kittler, M. Oehme, N. V. Abrosimov, O. F. Vyvenko, E. Kasper, and J. Schulze, Luminescence from germanium and germanium on silicon, *Solid State Phenomena* **205**, 383 (2014).
- [66] M. Kittler, T. Arguirov, M. Oehme, Y. Yamamoto, B. Tillack, and N. V. Abrosimov, Photoluminescence study of ge containing crystal defects, *physica status solidi (a)* **208**, 754 (2011).
- [67] F. Pezzoli, F. Isa, G. Isella, C. V. Falub, T. Kreiliger, M. Salvalaglio, R. Bergamaschini, E. Grilli, M. Guzzi, H. von Känel, *et al.*, Ge crystals on si show their light, *Physical Review Applied* **1**, 044005 (2014).
- [68] K. Tanaka, M. Suezawa, and I. Yonenaga, Photoluminescence spectra of deformed si-ge alloy, *Journal of applied physics* **80**, 6991 (1996).